Acta Oceanol. Sin., 2021, Vol. 40, No. 7, P. 129–141
https://doi.org/10.1007/s13131-021-1727-0
http://www.aosocean.com
E-mail: ocean2@hyxb.org.cn

Modelling the annual cycle of landfast ice near Zhongshan Station, East Antarctica

Jiechen Zhao[1, 2*], Tao Yang[3], Qi Shu[2, 4], Hui Shen[1], Zhongxiang Tian[1], Guanghua Hao[1], Biao Zhao[2, 4]

[1] Key Laboratory of Marine Hazards Forecasting, National Marine Environmental Forecasting Center, Ministry of Natural Resources, Beijing 100081, China

[2] Laboratory for Regional Oceanography and Numerical Modeling, Pilot National Laboratory for Marine Science and Technology (Qingdao), Qingdao 266237, China

[3] 92682 Unit, Zhanjiang 524001, China

[4] First Institute of Oceanography, Ministry of Natural Resources, Qingdao 266061, China

Received 24 March 2020; accepted 12 September 2020

Abstract

A high resolution one-dimensional thermodynamic snow and ice (HIGHTSI) model was used to model the annual cycle of landfast ice mass and heat balance near Zhongshan Station, East Antarctica. The model was forced and initialized by meteorological and sea ice *in situ* observations from April 2015 to April 2016. HIGHTSI produced a reasonable snow and ice evolution in the validation experiments, with a negligible mean ice thickness bias of (0.003±0.06) m compared to *in situ* observations. To further examine the impact of different snow conditions on annual evolution of first-year ice (FYI), four sensitivity experiments with different precipitation schemes (0, half, normal, and double) were performed. The results showed that compared to the snow-free case, the insulation effect of snow cover decreased bottom freezing in the winter, leading to 15%–26% reduction of maximum ice thickness. Thick snow cover caused negative freeboard and flooding, and then snow ice formation, which contributed 12%–49% to the maximum ice thickness. In early summer, snow cover delayed the onset of ice melting for about one month, while the melting of snow cover led to the formation of superimposed ice, accounting for 5%–10% of the ice thickness. Internal ice melting was a significant contributor in summer whether snow cover existed or not, accounting for 35%–56% of the total summer ice loss. The multi-year ice (MYI) simulations suggested that when snow-covered ice persisted from FYI to the 10th MYI, winter congelation ice percentage decreased from 80% to 44% (snow ice and superimposed ice increased), while the contribution of internal ice melting in the summer decreased from 45% to 5% (bottom ice melting dominated).

Key words: landfast ice, annual cycle, snow influence, Zhongshan Station, East Antarctica

Citation: Zhao Jiechen, Yang Tao, Shu Qi, Shen Hui, Tian Zhongxiang, Hao Guanghua, Zhao Biao. 2021. Modelling the annual cycle of landfast ice near Zhongshan Station, East Antarctica. Acta Oceanologica Sinica, 40(7): 129–141, doi: 10.1007/s13131-021-1727-0

1 Introduction

The snow cover on sea ice persists during most of the year in Antarctica (Arndt et al., 2016). Windblown redistribution is a key factor affecting the snow thickness distribution because of persistent strong winds over Antarctic sea ice, typically following precipitation events (Massom et al., 1997). As a result, snow thickness on the Antarctic sea ice may not be directly related to either the frequency or duration of snowfall (Massom et al., 2001). Therefore, the parameterization of snow accumulation in Antarctica from precipitation data is quite challenging, and the role of real snow cover on the evolution of ice thickness is not fully studied.

Snow plays a critical role in controlling the Antarctic sea-ice mass balance. Snow enhances the sea-ice surface reflectivity for incoming shortwave radiation and determines the amount of light being reflected, absorbed, and transmitted to the upper ocean (Arndt et al., 2016). However, precipitation rate sensitivity experiments with a dynamic-thermodynamic sea ice model have indicated that with present-day precipitation rates, the snow effect on the sea ice in Southern Ocean is dominated by snow-ice and/or superimposed-ice formation rather than the snow's insulation effect (Powell et al., 2005). Furthermore, regional model simulations revealed that the insulation effect of snow dominates the factors influencing maximum ice thickness in the landfast sea ice zone near Zhongshan Station, especially near the coastline area (Zhao et al, 2019a).

Snow contributes significantly to the sea ice mass balance because of widespread surface flooding and related snow-ice formation (Arndt et al., 2016). Large-scale estimation, using passive microwave products, shows that snow ice is largely ubiquitous in all regions throughout the growth season, but snow ice production is largely independent of snow depth (Maksym and Markus, 2008). A summer drift experiment in the Weddle Sea found that snow on the second-year ice was thicker, colder, denser, and more layered than on the first-year ice (FYI). Ice freeboard was mostly negative, but flooding occurred mostly on the first-year ice (Nicolaus et al., 2009).

In the Prydz Bay, landfast ice exists from February to December and breaks up every year during the short time in summer. Field observations have shown that snow contributes to the

Foundation item: The National Natural Science Foundation of China under contract Nos 41876212, 41911530769 and 41676176.
*Corresponding author, E-mail: zhaojc@nmefc.cn

thickness of the multi-year ice (MYI) near Zhongshan Station through the formation of snow ice and superimposed ice (Tang et al., 2006). The maximum first-year ice thickness ranges from 1.4 m to 1.8 m by the end of October, accompanied by variable thick snow cover (Lei et al., 2010; Zhao et al., 2017; Yu et al., 2019). Inside the Nella Fjord, 3.0-m thick multi-year ice has been observed with a 1.0-m thick snow cover, which indicates that superimposed ice from snow melting and refreezing contributes to ice thickness (Zhao et al., 2019b). Long-term records from the Australian Davis Station showed an upward trend of 3 mm/a in total solid precipitation from 1977 to 2002. The cumulative solid precipitation and annual maximum ice thickness showed a significant trend of lower ice thickness with increasing precipitation owing to the competing effects of snow insulation in winter. The records from Davis also showed a trend toward delayed ice breakout date of +0.43 d/a (Heil, 2006). Analysis of a multi-source observation datasets near Zhongshan Station revealed a negative relationship between mean snow and maximum landfast ice thickness, revealing the insulation effect of snow on landfast ice evolution (Zhao et al, 2019a).

Modeling studies have been carried out for Antarctic fast ice. Crocker and Wadhams (1989) modeled fast ice in the McMurdo Sound with modifications to Arctic models to include snow ice and platelet ice in the ice stratigraphy. Yang et al. (2016a) modeled the annual cycle of fast ice thickness in the Prydz Bay applying a high resolution one-dimensional thermodynamic snow and ice (HIGHTSI) model (Launiainen and Cheng, 1998). The same model was used to study the different evolutions of thickness of FYI and MYI near Zhongshan Station (Zhao et al., 2017) and the influence of snow on year-round ice evolution in the Prydz Bay (Zhao et al., 2019a).

Snow thickness was spatially and temporally nonhomogeneous near Zhongshan Station. In some seasons, no snow or thin snow was observed (Lei et al., 2009, 2010). However, long-term observations have shown that solid precipitation was frequent and snow thickness can be up to 0.5–1.0 m on the ice surface near Zhongshan Station in some seasons (Zhao et al., 2019a, b). The annual cycle of landfast ice in the Prydz Bay has been studied by considering a snow-free condition on the ice surface (Yang et al., 2016a). In this study, a HIGHTSI model was used to further investigate the ice mass and heat balance, focusing on the influence of snow cover on the early ice growth season and the onset of surface melt, which was the main difference from Zhao et al. (2019a). Additionally, even MYI was not often occurred near Zhongshan Station (Heil, 2006; Lei et al., 2010), but it was observed in some specific year (Zhao et al., 2017). Therefore, the investigation of snow effect on MYI was another important attempt in this paper. The model and experiments are introduced in Section 2. Results are shown in Section 3. The discussion and conclusions are presented in Sections 4 and 5, respectively.

2 Materials

2.1 *Model*

The HIGHTSI model was initially developed to calculate seasonal snow and ice thermodynamics for the boreal lake and Baltic Sea (Launiainen and Cheng, 1998; Cheng et al., 2003, 2006), and has been further developed to investigate snow and ice thermodynamics in the polar regions (Cheng et al., 2008; Yang et al., 2012, 2016a; Zhao et al., 2017, 2019a). The HIGHTSI model includes the full description of the detailed interactions between snow, slush, and ice, which was usually ignored in the community sea ice-ocean coupled model. In summer, the fresh water from snow melt produces slush, and may further freezes to ice if the temperature drops to zero during the night or the cold air events. Thick snow accumulation induced by large snowfall events may cause the negative freeboard. Sea water floods into snow layer and produces salty slush, which may also freezes to ice when the temperature drops to the freezing point. The parameterization of the transformation from snow to ice (snow ice and superimposed ice) is very important for sea ice simulation in Antarctica and those processes contribute more to the ice mass balance. Except for bottom and surface melting, internal melting may be an important factor for summer ice, when the internal ice temperature is high enough to melt inside. The detailed description about the HIGHTSI model can be found in Cheng et al. (2014). A previous study by Yang et al. (2016a) has suggested that HIGHTSI model has a reliable ability to reproduce sea ice evolution under snow-free conditions near Zhongshan Station, which is the same region as in this study.

2.2 *Observations*

The primary external forcing needed by the HIGHTSI model includes wind speeds (V_a), air temperature (T_a), relative humidity (Rh), cloud fraction (CN), precipitation ($Prec$), and oceanic heat flux (F_w). In this study, V_a, T_a, and Rh came from the observations of automatic weather station at Zhongshan Station, which were recorded at 1-min intervals. CN was manually recorded every 6 h by a professional observer at Zhongshan Station. $Prec$ was measured daily at Progress Station, which is about 1 km southeast of Zhongshan Station, as shown in Fig. 1b. The technical details of these meteorological observations can be found in Zhao et al. (2019a). All of the parameters were interpolated into hourly values, as required by the model.

During the study period from April 2015 to April 2016, the annual mean wind speed was 6.4 m/s and the maximum daily mean value was 27.6 m/s, recorded on 2 September (Fig. 2a). The annual mean air temperature was –11.2°C and the maximum and minimum daily mean values were 7.8°C (December 21, 2015) and –39.9°C (July 8, 2015) (Fig. 2b). The mean relative humidity was 59.9% (Fig. 2c). The cloudiness was high in winter and low in summer (Fig. 2d). Precipitation was rare during December and January, but significant in other months (Fig. 2e). Oceanic heat flux (F_w) is a parameter with much uncertainties. The previous study at Davis Station (about 100 km northeast of Zhongshan Station) showed that seasonal F_w ranges from 0 to 18 W/m^2 (Heil et al., 1996). An estimation based on observations at Zhongshan Station by Lei et al. (2010) showed that F_w decreased from 12 W/m^2 in April to 2 W/m^2 in September, then increased sharply to 20 W/m^2 in the end of the year. The estimation from a thermodynamic snow/ice model suggested that F_w at Zhongshan Station decreased from about 25 W/m^2 in April to 5 W/m^2 toward the end of the year (Yang et al., 2010). The latest results based on residual method showed an annual cycle of F_w from about 30 W/m^2 during March–May, about 10 W/m^2 during August–October, and about 15 W/m^2 in November for the year 2012 at Zhongshan Station (Zhao et al., 2019a). The time series of F_w used for this study was reestablished based on these previous studies, which decreased smoothly from around 30 W/m^2 in April to around 10 W/m^2 in December and then increased back to around 30 W/m^2 (Fig. 2f).

Snow and ice *in situ* observations were used as the initial conditions and to validate the model simulations. In 2015, Snow and Ice Mass Balance Array (SIMBA) buoy was deployed near Zhongshan Station (Fig. 1b), which has a 4.8-m long temperature chain with 240 sensors at 0.02 m intervals. The buoy recorded vertical

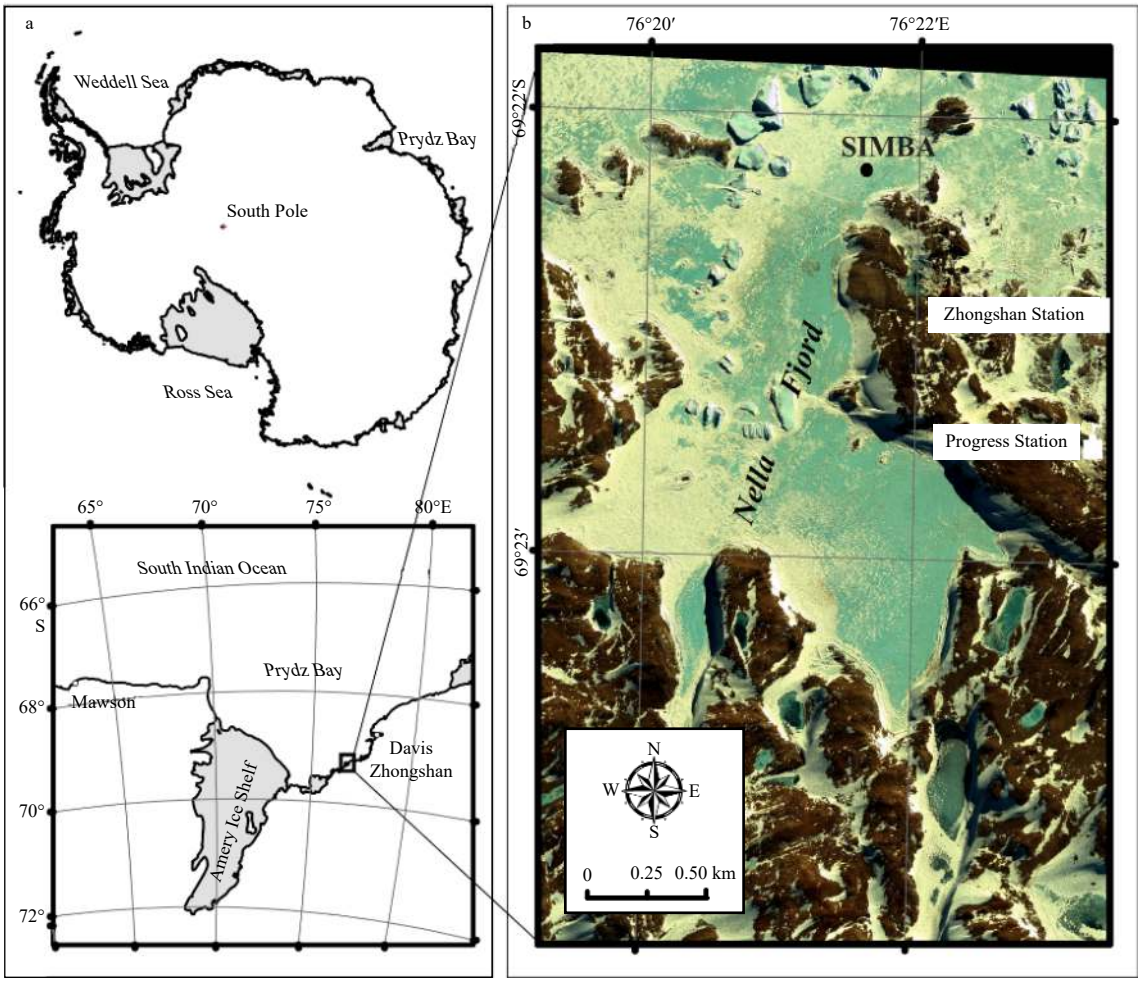

Fig. 1. The location of Prydz Bay and Zhongshan Station (a), and a satellite image of the area around Zhongshan Station (b). The Snow and Ice Mass Balance Array (SIMBA) buoy was deployed near the landfast ice observation site, which is marked by a black dot.

snow and ice temperature profiles every 6 h. The manual observations were carried out throughout the entire winter. Ice holes were drilled once a week around the SIMBA site and ice thickness was measured with an ice gauge. Snow thickness was measured with a stainless steel ruler (Zhao et al., 2019a).

2.3 *Experiments*

To validate the model performance, a simulation was run for April 15 to December 15, 2015 (Exp. V), the same time period as the *in situ* observations. The initial ice thickness was 0.3 m, and snow thickness was prescribed based on *in situ* records.

To better understand the annual cycle of FYI and examine the sensitivity of ice evolution to snow thickness, Exps F1–F4 were designed with the same external forcing and other setup parameters as Exp. V, but different precipitation schemes (Table 1). These four simulations started on April 15, 2015 and ran for one year.

In addition, Exp. MYI was designed to examine the annual cycle of MYI, starting on April 15, 2015. Even MYI have ever observed in the Nella Fjord (Zhao et al., 2019a), but age of those MYI floes was unknown because of the short of systemic and continuous observations. In order to fully investigate the mass balance, especially the equilibrium state of MYI, the run time was set to 10 years in this study. The external forcing was the repetition of the FYI experiment and precipitation scheme was the normal condition.

The parameterization of snow thickness in this paper was based on the accumulation of solid precipitation. However, this study designed sensitivity experiments with different precipitation schemes and snow thickness to reproduce the scenes of snow redistribution by wind. The reason for avoiding to directly consider the windblown snow effect in the model code, were the rare knowledge of the complicated processes.

The albedo parameterization in the HIGHTSI model played an important role in the simulations of snow/ice surface heat balance, but large uncertainties still existed because of limited field observations (Yang et al., 2016b). To further examine the influence of different albedo parameterizations on the model results, three different albedo schemes were used for an inter-comparison analysis, using the same external forcing as Exp. F3. The default albedo scheme used in this study was developed by Lynch et al. (1995). This medium complexity scheme considers surface temperature, snow, and ice thickness (A1, Table 2). A low complexity scheme by Parkinson and Washington (1979) uses constant broadband albedo for snow and bare ice (A2, Table 2). A high complexity scheme by Briegleb et al. (2004) uses weighted albedos with snow and ice thickness and also considers visible and near-infrared albedos (A3, Table 2).

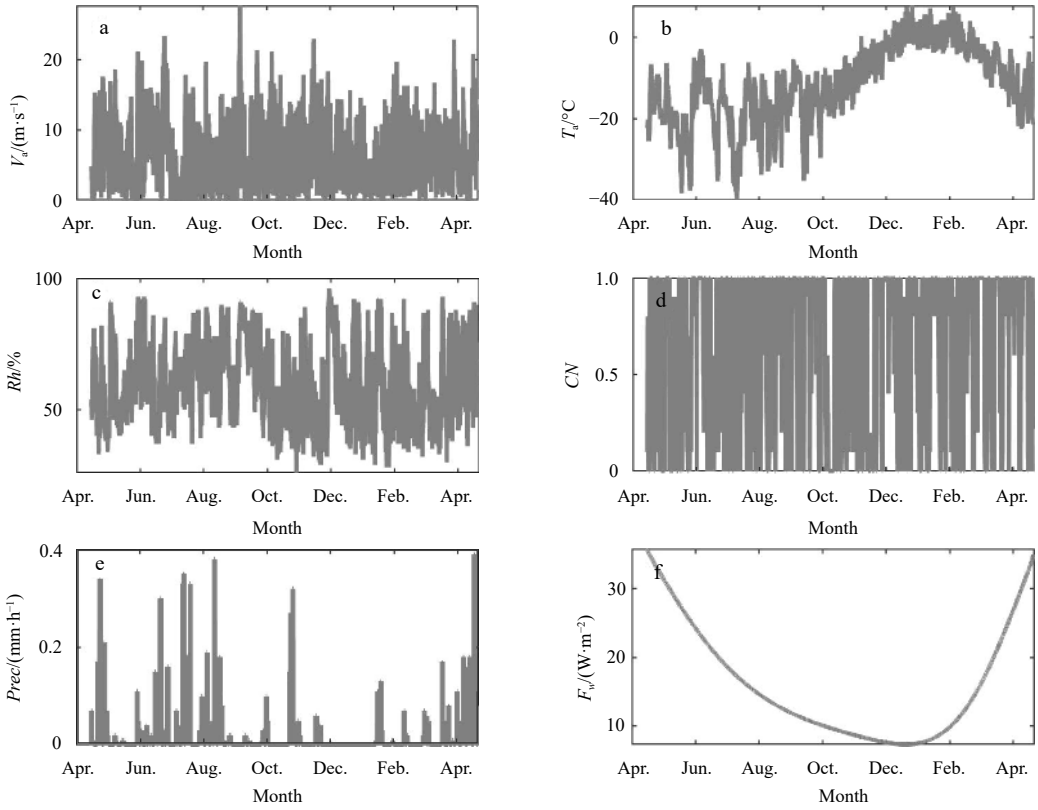

Fig. 2. The hourly external forcing used for HIGHTSI model from April 2015 to April 2016: wind speed (a), air temperature (b), relative humidity (c), cloud fraction (d), precipitation rate (e), and oceanic heat flux (f).

Table 1. Descriptions of FYI sensitivity experiments with different precipitation schemes

Exp. name	Start time/a	Run time/a	Initial ice thickness/m	Initial snow thickness	Precipitation scheme
F1	15 April	1	0.3	0	0
F2	15 April	1	0.3	0	half *Prec*
F3	15 April	1	0.3	0	normal *Prec*
F4	15 April	1	0.3	0	double *Prec*

3 Results

3.1 *Validation experiment results*

The snow and ice temperature evolution recorded by the SIMBA buoy is shown in Fig. 3a. The evolution of snow and ice temperature modeled in Exp. V is shown in Fig. 3b. Surface snow temperatures can decrease to –25°C during April–October, leading to a large temperature gradient in the ice. HIGHTSI produced a reasonable temperature response to the air temperature change, similar to the SIMBA observations. The black dots in Fig. 3 represent *in situ* ice thickness observed by manual drilling.

Table 2. Detail descriptions of three albedo schemes used in the albedo sensitivity experiments. The symbols H_i and H_s represent ice and snow thickness. The symbols T_{is} and T_m represent ice surface temperature and ice melt point. The symbols vs and ni represent visible and near-infrared albedos. The symbol T_{ss} represents snow surface temperature

Albedo scheme	Formula for ice and snow albedo
A1	$alb\_i \sim (H_i T_{is} T_m)$; $alb\_s \sim (alb_i H_s T_{is})$
A2	alb_i=0.6; alb_s=0.8
A3	$alb\_i \sim \left(alb_i^{vs} alb_i^{ni} H_i T_{is}\right)$; $alb\_s \sim \left(alb_s^{vs} alb_s^{ni} T_{ss}\right)$

Modeled ice thickness matched well with observations, with a high correlation coefficient of 0.99 and mean deviation of (0.003±0.06) m. The model predicted slow growth in May and June (0.3 cm/d) and rapid growth in July (1.0 cm/d), which was related to the insulation effect of thick snow cover in May and June. This comparison of the model results with observed parameters confirms that HIGHTSI can accurately predict the evolution of ice when there is thick snow cover on the ice surface.

3.2 *FYI experiment results*

The results of the modeled annual cycle of FYI snow and ice evolution are shown in Fig. 4 for four different precipitation schemes. For all of the four experiments, the snow and ice temperature gradient was larger during the ice growing season from April to November and smaller in the melting season. The insulating effect of the snow cover was obvious. The temperature gradient in ice was much smaller when snow cover existed than the snow-free case. When air temperature declined during the second winter, snow cover prevented the ice column from freezing quickly. These conditions maintained the isothermal condition in the lower part of ice column and prolonged bottom melting until the end of March in the second year. In early February, ice thickness was nearly zero in the snow-free case and around

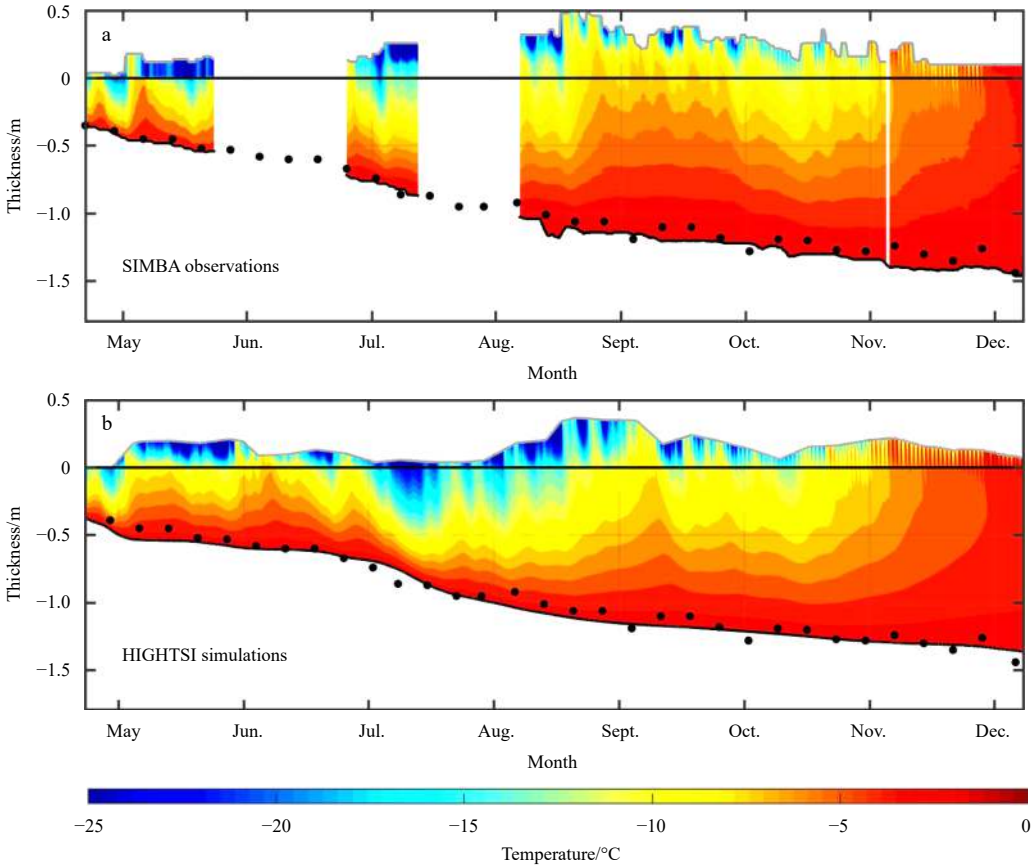

Fig. 3. The snow and ice temperature profile observed by Snow and Ice Mass Balance Array (SIMBA) buoy (a) and simulated by HIGHTSI in Exp. V (b), from 15 April to December 15, 2015. In a, the snow surface and ice bottom was detected from SIMBA temperature profiles by a semi-automatic algorithm (Zhao et al., 2017). The zero position represents the snow/ice interface. The black dots represent the observed *in situ* ice thickness.

one meter in the snow cover cases, which indicates that it was easier for ice to melt away or break up in the summer without the protection of snow cover.

In general, maximum snow thickness increased with increasing precipitation (Fig. 5a). From Exp. F3 to F4, the precipitation doubled, but the corresponding increase of snow thickness was less than double because thick snow cover (Fig. 4) caused much more flooding, leading to much more snow-to-ice transformation. The maximum ice thickness for Exps F1–F4 was 1.67 m, 1.35 m, 1.23 m, and 1.42 m, respectively (Fig. 5b). Snow cover delayed ice melting by about one month, compared to the snow-free scenario. Thick snow cover caused a negative freeboard in winter, leading to the flooding of sea water into snow layers (Fig. 5c). Albedo was also sensitive to snow surface melting. The albedo deceased significantly when snow melt began in summer. In the winter, snow cover increased the surface albedo by 0.1–0.2, compared to the snow-free case (Fig. 5d).

The accumulated ice bottom growth decreased as snow thickness increased (Fig. 6a). Thicker snow cover leads to a greater insulation effect, a smaller ice temperature gradient, and thus a smaller growth rate. The ice bottom freezing contributed 100% (Exp. F1), 95% (Exp. F2), 80% (Exp. F3), and 44% (Exp. F4) of the total ice gain. Snow ice formed in the thick snow cases of Exps F3 and F4 (Fig. 6b). According to the Archimedes principle, thick snow cover on a thin ice would lead to a negative freeboard and flooding of sea water into the snow layer. Snow mixed with sea water was considered to be slush in the model and froze to snow ice if the temperature was low to freezing point. In Exps F3 and F4, accumulated snow ice was 0.19 m and 0.69 m, respectively accounting for 12% and 49% of the maximum ice thickness. Superimposed ice formed in summer in Exps F2–F4 (Fig. 6c). Beginning in November, increased air temperature and strong solar radiation started to melt snow cover. Snow surface melt decreased albedo and enhanced solar radiation absorption, which triggered positive feedback and more surface snow cover melted. Melting snow first became slush and then froze to fresh ice when the temperature dropped to zero at night. This kind of ice derived from melting snow was named superimposed ice. The accumulation of superimposed ice was 0.07–0.14 cm, accounting for 5%–10% of the maximum ice thickness in Exps F2–F4. For the snow-free case, no superimposed ice or snow ice formed, but ice surface suffered a significant melting of 0.1 m (6% of the total ice loss) in summer (Fig. 6d). Internal melting occurred in all the experiments and was especially large in the snow-free case, up to 0.93 m, which accounted for 56% of the total ice loss in summer (Fig. 6e). The percentage of internal melting was smaller in the thick snow case, close to the 35% seen in the double precipitation experiment (Exp. F4).

3.3 *MYI experiment results*

The MYI 10-year simulations tried to reproduce the transform processes of FYI to MYI near Zhongshan Station. Snow

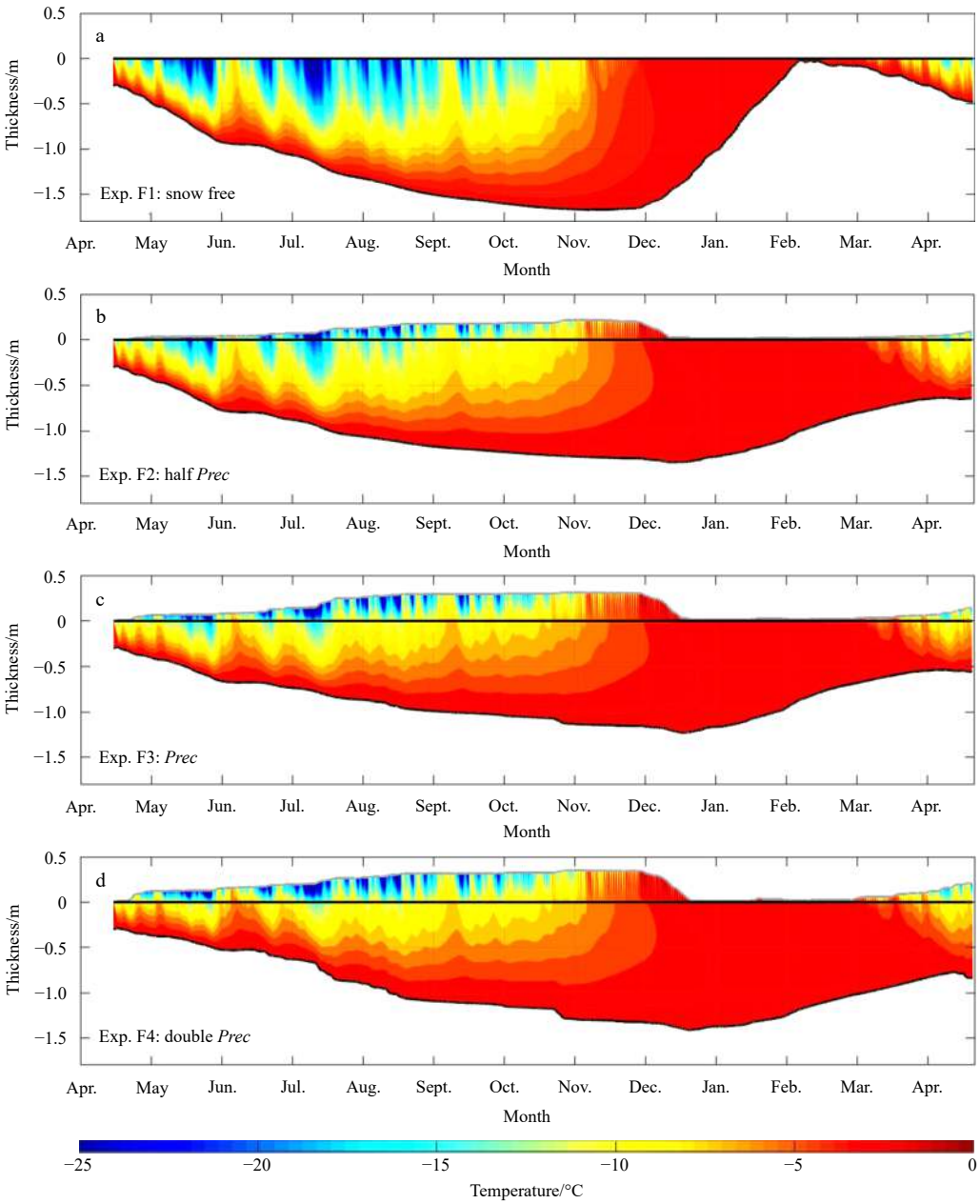

Fig. 4. Snow and ice temperature profiles from April 15, 2015 to April 15, 2016 for Exp. F1 (a), Exp. F2 (b), Exp. F3 (c), and Exp. F4 (d). The zero position represents the snow/ice interface.

thickness showed a significant seasonal and inter-annual cycle, and the maximum snow thickness increased year by year (Fig. 7a). Ice thickness also showed a significant seasonal cycle and an increasing inter-annual trend. The maximum ice thickness increased from 1.24 m in the first year to 1.99 m in the 10th year. From the 7th year on, the annual evolution of ice thickness seemed to reach an equilibrium, with a maximum of 1.99 m in December/January and a minimum of 1.40 m in March/April (Fig. 7b). In the 10th year, freeboard was negative during the entire annual period, suggesting a continuous production of snow ice all year (Fig. 7c). The increase of both snow and ice thickness contributed to a greater albedo in the 10th year than in the 1st year. This prevented summer ice underneath snow cover from melting, perhaps strengthened the stability of MYI (Fig. 7d).

Yearly accumulations are displayed in Fig. 8. Snow ice ranged between 0.14 m and 0.27 m in the 10-year simulations. The bottom ice freezing reached a maximum of 0.73 m in the 1st year and gradually decreased to 0.31 m in the 10th year. Superimposed ice increased slightly over 10 years, from 0.12 m to 0.22 m. Bottom ice melting reached an equilibrium of 0.61 m in the last few years and internal ice melting decreased significantly from 0.34 m in the 1st year to 0.03 m in the 10th year.

The results showed that congelation ice from bottom freezing dominated the total ice gain (80%) during the 1st year ice but gradually declined its importance (44%) in the 10th year. Therefore, congelation ice was the main component of FYI, while nearly equal to snow ice and superimposed ice in MYI. In this 10-year simulations, no surface ice melting occurred because of the existence of thick snow cover. The results showed that internal melting accounted for 45% of total ice loss of the 1st year ice,

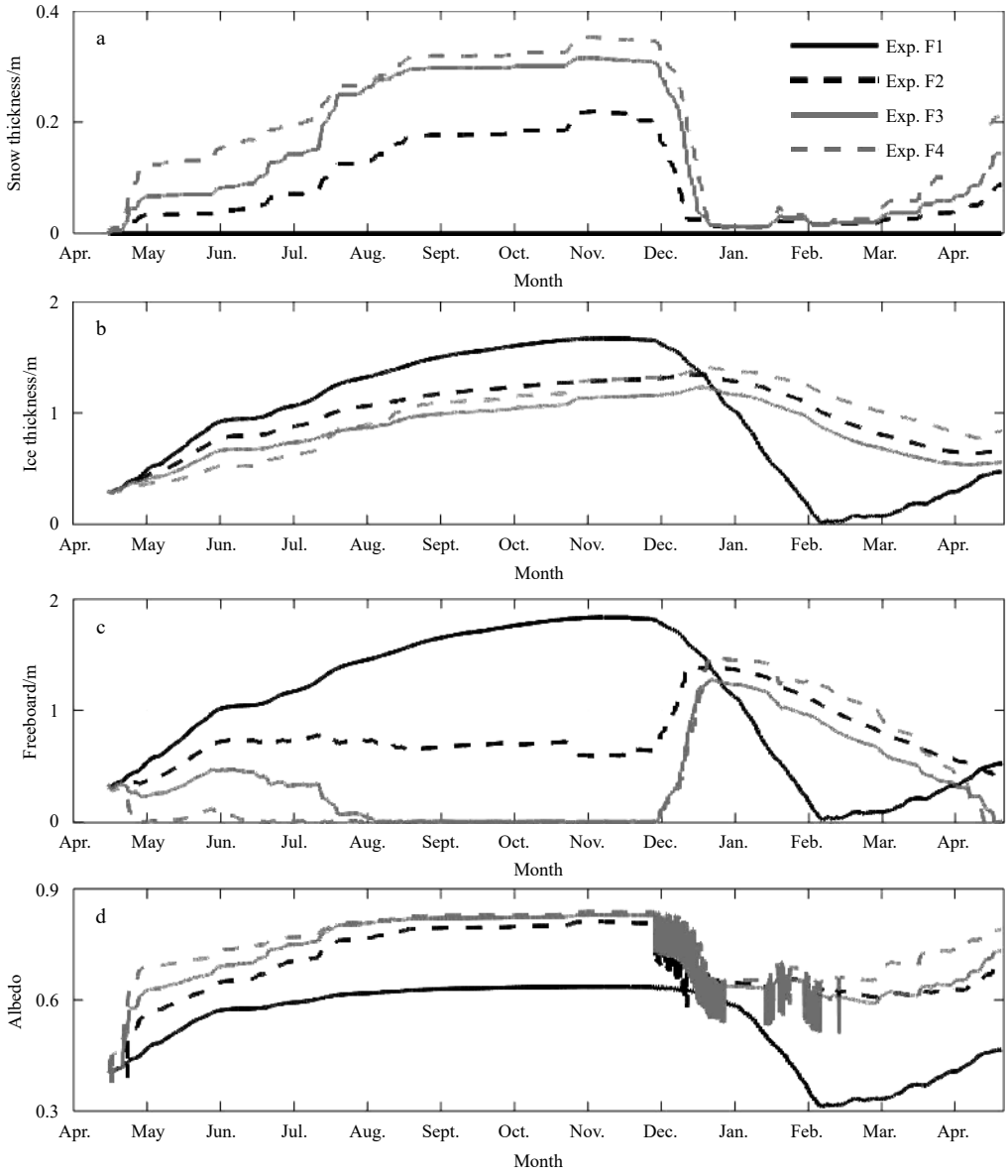

Fig. 5. Snow thickness (a), ice thickness (b), freeboard (c), and albedo (d) simulated from April 15, 2015 to April 15, 2016.

while decreased to 5% of the 10th year ice. Therefore, bottom melting dominated the summer melting of MYI with thick snow cover.

3.4 *Albedo experiment results*

The albedo scheme determines the amount of penetrating solar radiation and will influence the simulation results. Therefore another two albedo schemes were selected to conduct the inter-comparison experiments of albedo sensitivity (Table 2). Detailed descriptions of albedo schemes A1, A2, and A3 are given in Table 2. Albedo varied greatly among the three different schemes in the early winter and in the melting season. A1 was usually 0.1–0.2 smaller than A2 and A3 (Fig. 9a). The different albedo schemes had little influence on the snow and ice evolution in winter, but had a larger effect in summer. The smaller summer snow and ice thickness was modeled for A1, when low albedo resulted in more penetrating solar radiation (Figs 9b and c). Albedo schemes affected the amount of superimposed ice formation (about 10% among three schemes, Table 3) because of the different amounts of summer snow melting, and also slightly affected the amount of snow ice because of the different negative freeboard during winter (Fig. 9d). However, the largest difference was among internal ice melting, which was directly caused by the different summer solar penetration (Table 3).

4 Discussion

To further reveal the effect of snow cover on sea ice mass balance in this study, some extra sensitive experiments were designed to quantify the effect of different precipitation and melt schemes (0, half, normal and double) during the early ice growth season (April–May), and the onset of surface melt (November–December). Normal precipitation forcing was used for the other periods, but different precipitation schemes (0, half, normal and double) were designed during the early ice growth season (15 April–15 May) for Exp. S, and a different snow melt rate schemes (0, half, normal and double) during the onset of surface melt (15 November–15 December) for Exp. M. The other setup and forcing were the same as the FYI experiments.

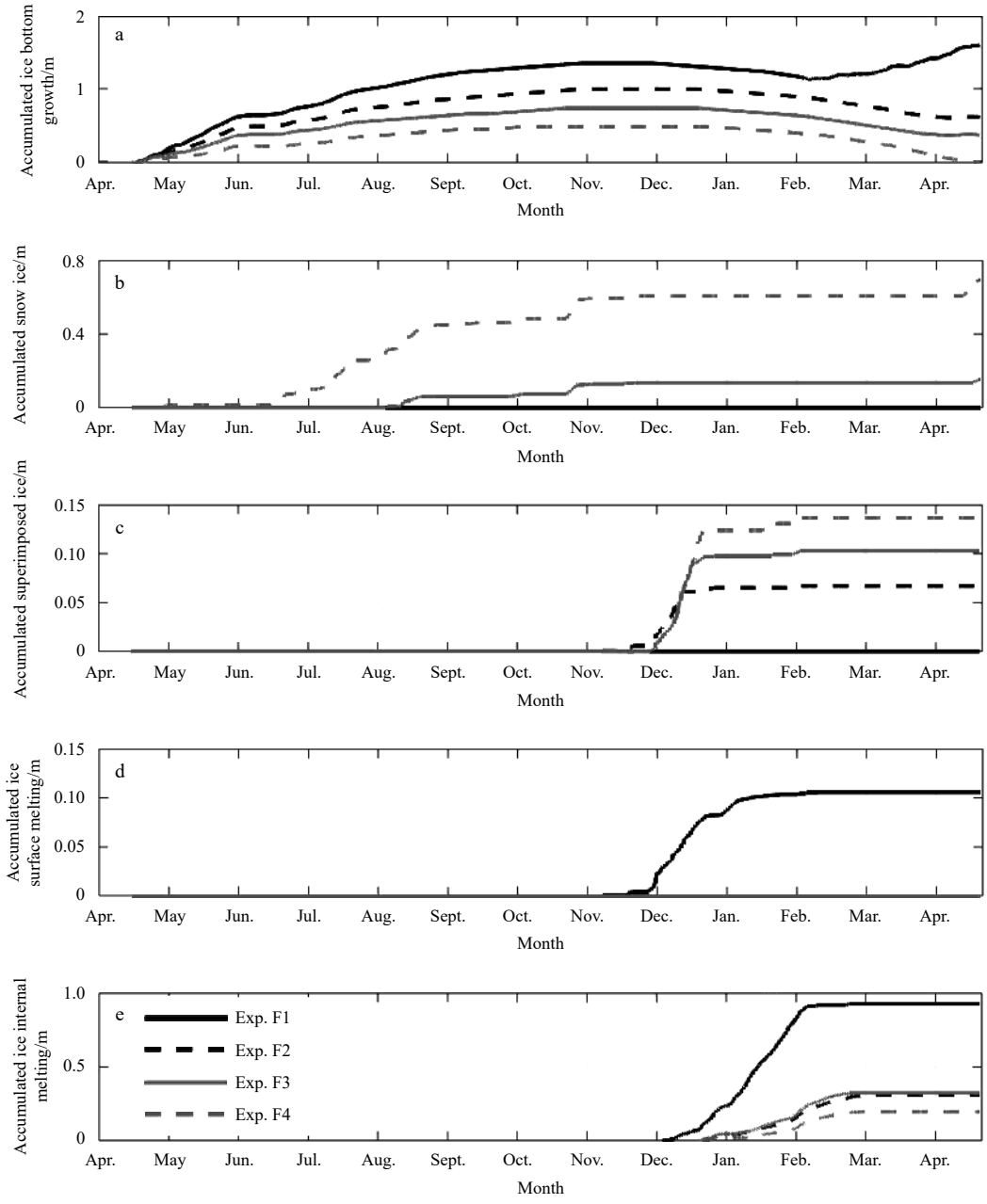

Fig. 6. Accumulated ice bottom growth (a), accumulated snow ice (b), accumulated superimposed ice (c), accumulated ice surface melting (d), and accumulated ice internal melting (e) from April 15, 2015 to April 15, 2016.

Different precipitation schemes (0, half, normal and double) during the early ice growth season (15 April–15 May) influenced ice mass balance significantly, as shown in Fig. 10. The ice surface temperature were –15.6°C, –12.6°C, –10.7°C, –8.4°C, respectively for Exps S1–S4, because the insulation effect of snow cover led to higher ice surface temperature. The smaller vertical temperature gradient led to smaller ice bottom freezing, for example, the ice thickness on 15 May were 0.67 m, 0.57 m, 0.50 m, 0.41 m, respectively for Exps S1–S4. Therefore, during 15 April–15 May, double precipitation scheme reduced 39% ice mass, compared to the zero precipitation scheme. This reduction extended throughout the entire ice season, and brought a 8%–19% decrease to annual maximum ice thickness for half–double precipitation schemes (Exps S2–S4).

Snow played an important role on the timing of ice surface melt and further annual maximum ice thickness. When snow melt rate increased from half (Exp. M2, Fig. 11b) to double (Exp. M4, Fig. 11b), the timing of ice surface melt stated earlier, from Julian day 351 to 337, and in the meantime, annual maximum ice thickness came earlier, from Julian day 353 to 340. The maximum ice thickness also affected by the different melt rate schemes, which was 1.29 m and 1.19 m, respectively for half and double schemes.

The two groups of sensitivity experiments Exp. S and Exp. M brought us two facts: (1) snow conditions during the early ice growth season largely affected ice mass balance, then further determined the annual maximum ice thickness; (2) snow conditions during the onset of surface melt influenced the length of growth season, and thick snow would delay the timing of surface melt.

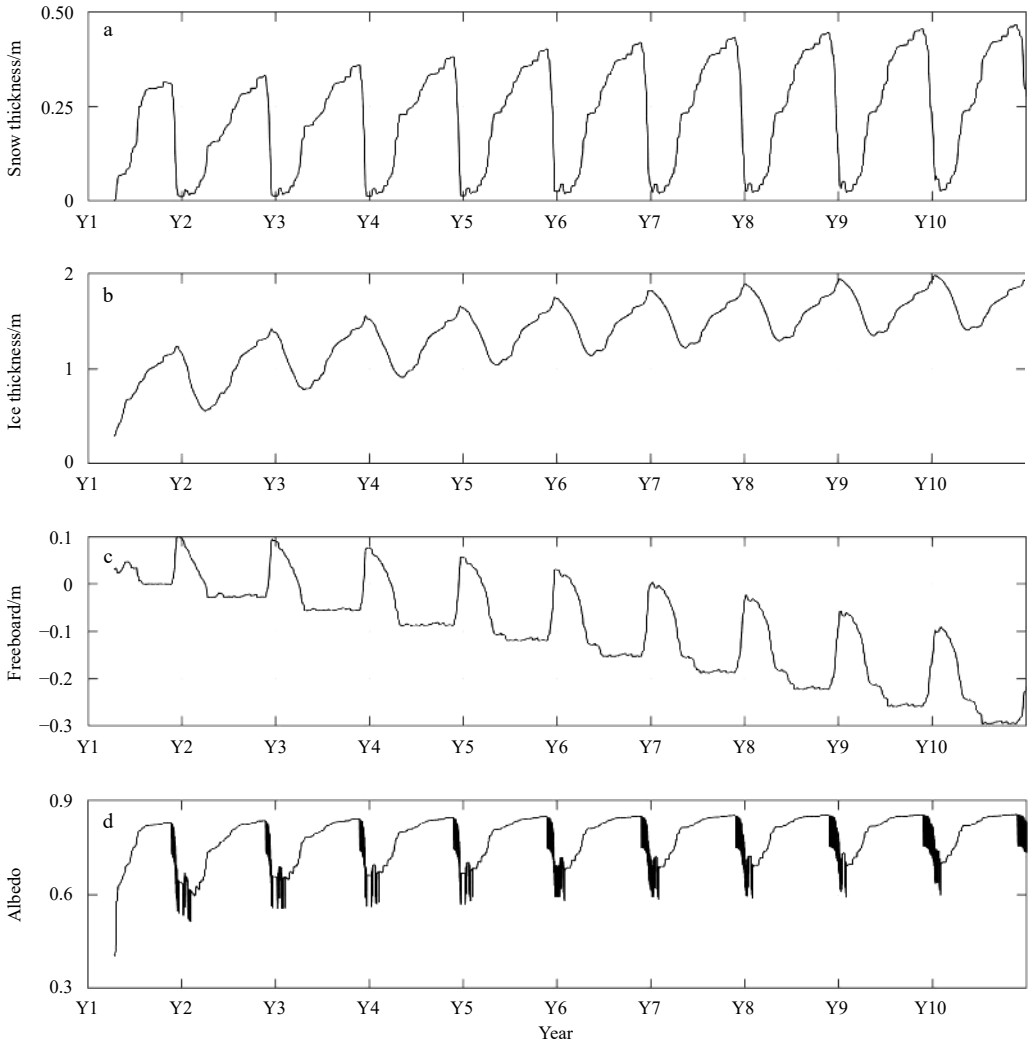

Fig. 7. Snow thickness (a), ice thickness (b), freeboard (c), and albedo (d) in the 10-year simulations for Exp. MYI.

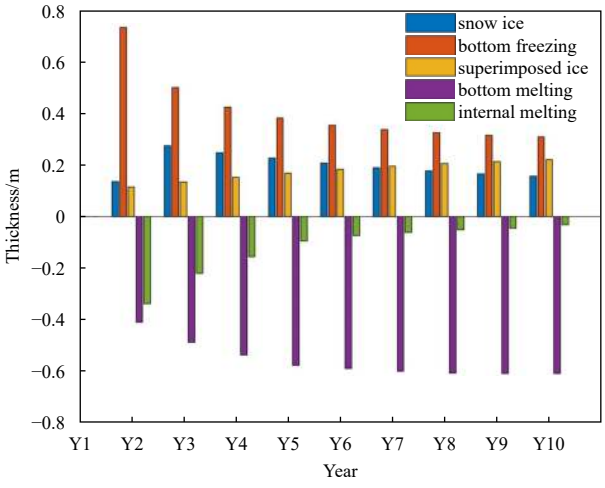

Fig. 8. Yearly accumulations of snow ice, bottom freezing, superimposed ice, bottom melting and internal melting in the 10-year simulations for Exp. MYI. Ice gain was positive and ice loss was negative in this figure.

For all the experiments in this paper, only thermodynamic processes of landfast ice was considered and simulated. In fact, dynamic processes was also important for landfast ice, like its breakup in summer, even in winter along with strong wind or tide. For example, tidal cracks were reported to appear in the landfast ice region in winter (Zhao et al., 2020), indicating that dynamic processes may have an influence on atmosphere-ice-ocean heat and mass transformation in the landfast ice zone. However, it is quite difficult to quantize those complicated dynamic processes in this one-dimensional snow and ice model, due to the rare field observations and theoretical research.

5 Conclusions

The HIGHTSI model was used to investigate the annual cycle of landfast ice near Zhongshan Station, East Antarctica. A series of experiments were conducted in this study, including an eight-month validation experiment, a year-round FYI sensitivity experiments with different precipitation schemes (0, half, normal, and double), a 10-year MYI experiment, and albedo sensitivity experiments. Furthermore, two another groups of sensitivity experiments were designed to especially reveal the effect of snow cover during the early ice growth season (April–May), and the onset of surface melt (November–December). All of the simulations were forced by meteorological observations from Zhongshan Station

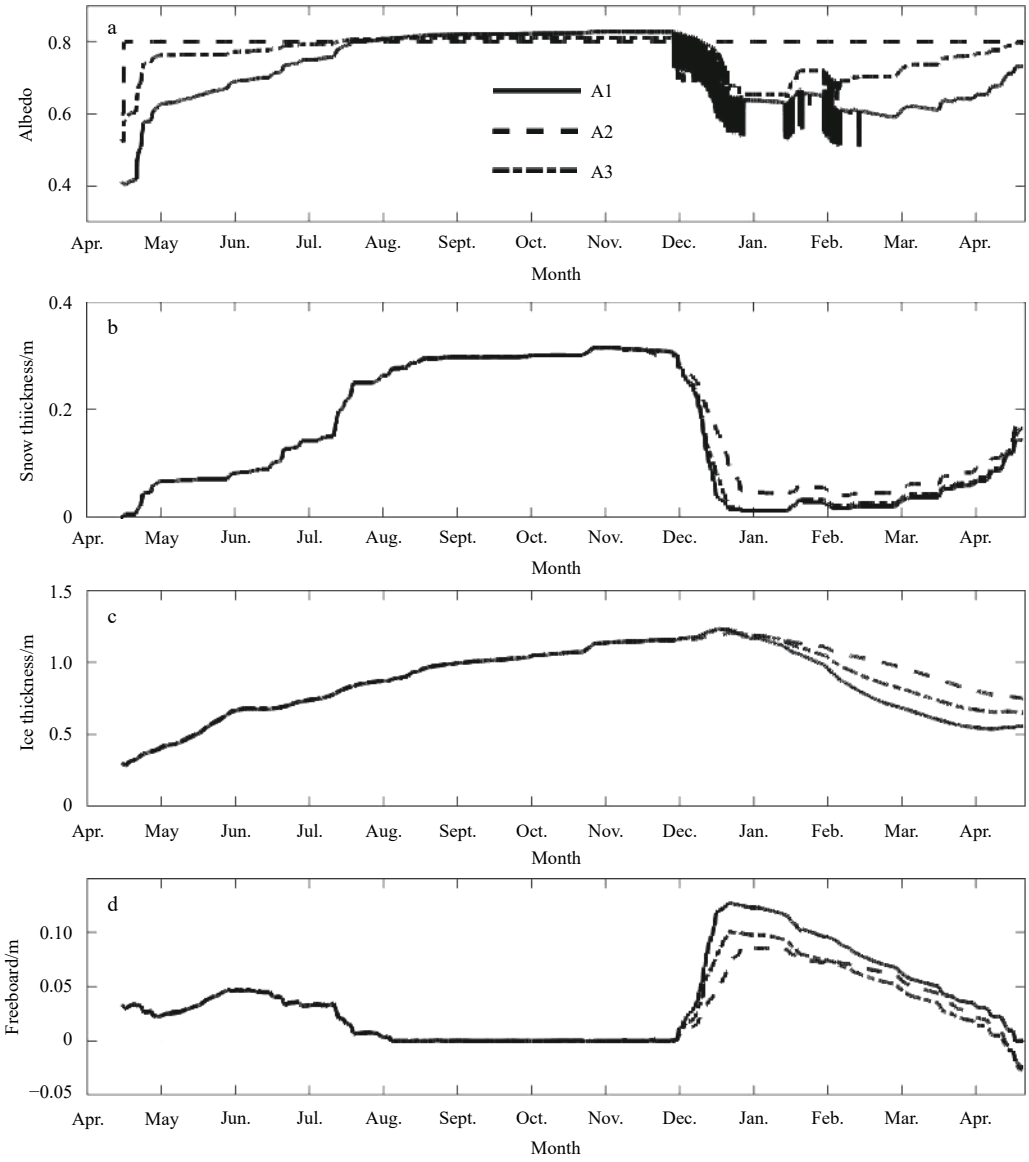

Fig. 9. Results of albedo sensitivity experiments: albedo (a), snow thickness (b), ice thickness (c), and freeboard (d). The model setup and forcing was the same as Exp. F3 except for albedo schemes.

Table 3. The statistic results from albedo sensitivity experiments

	A1	A2	A3
Maximum snow thickness	1.23	1.21	1.23
Maximum ice thickness	0.32	0.32	0.32
Accumulated ice bottom growth	0.37	0.33	0.35
Accumulated snow ice	0.13	0.09	0.09
Accumulated superimposed ice	0.10	0.11	0.11
Accumulated ice internal melting	0.34	0.10	0.22

and Progress Station. The *in situ* sea ice observations were used as the initial condition and validation materials. The results are summarized below.

Snow cover reduced the rate of bottom ice freezing in winter, because of its strong isolation effect. For example, compared to the snow-free case, the insulation effect of snow cover led to 15%–26% reduction of maximum ice thickness. Furthermore, 8%–19% was contributed by the influence during the early ice growth season (April–May). In the snow-free case, 100% of the ice column was derived from bottom freezing, whereas in the double precipitation experiment, the percentage decreased to 44%.

Thick snow cover on the thin ice column led to negative freeboard and snow ice formation during the winter. Nearly 50% of the total ice column was snow ice in the double precipitation experiment (Exp. F4). The melting of snow cover in summer caused superimposed ice formation, which accounted for 5%–10% of the maximum ice thickness in the FYI sensitivity experiments. The onset of ice melting was delayed for about one month when snow cover existed.

Internal melting was an important process, but hard to observe. The simulations showed that internal melting occurred in both the snow-free case and the thick snow case. Nearly 56% of the summer ice loss in the snow-free case was due to internal melting, but this percentage reduced to 35% in the double precipitation experiment (Exp. F4), because solar radiation was easier to come into ice in the snow-free case, but reflected largely in the thick snow conditions.

The 10-year simulation showed that the percentage of total

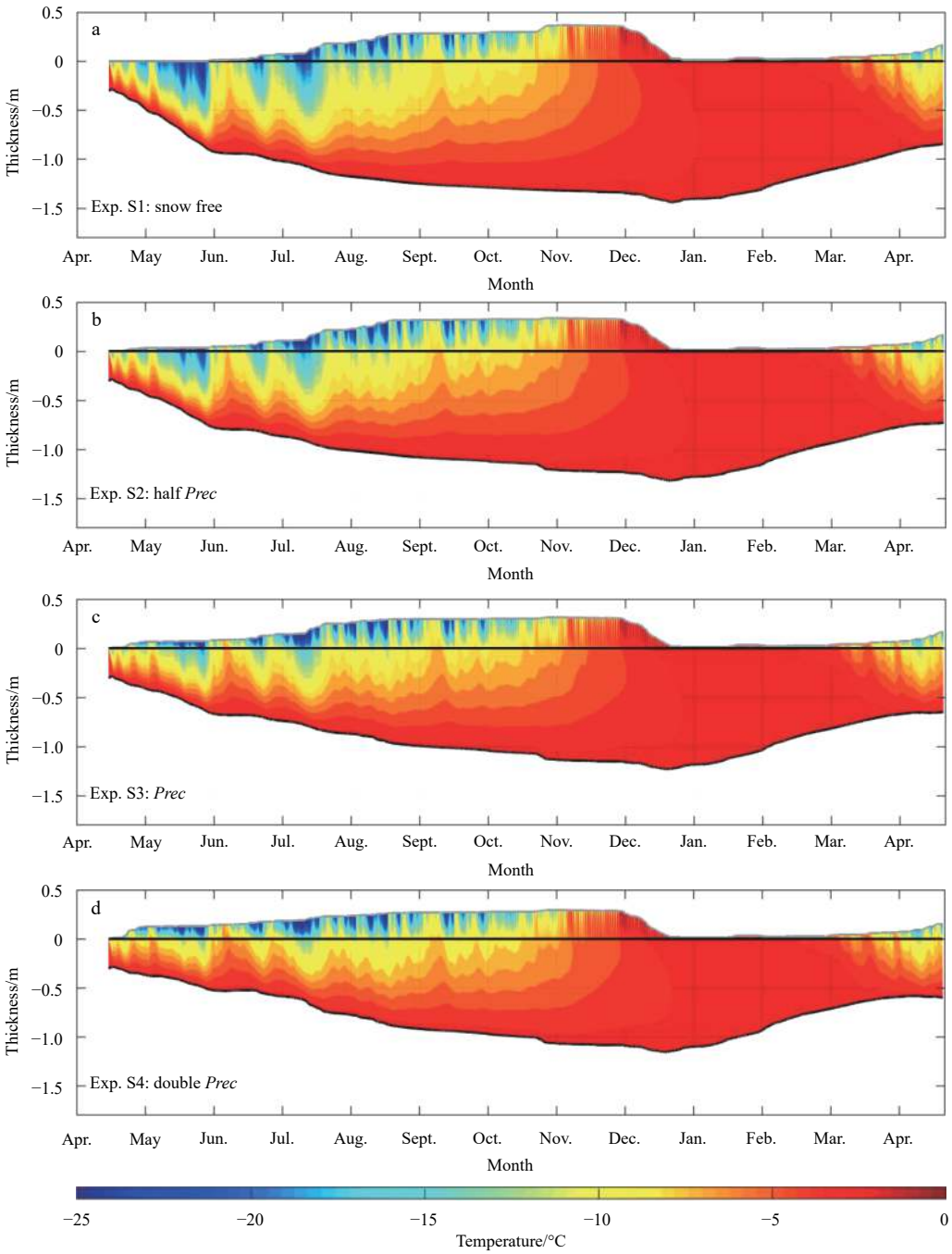

Fig. 10. Sensitivity experiments of different precipitation schemes for early ice growth season (15 April–15 May): Exp. S1 (a), Exp. S2 (b), Exp. S3 (c), and Exp. S4 (d). The zero position represents the snow/ice interface.

ice gain in winter from congelation ice (bottom freezing) decreased from 80% in the first year to 44% in the 10th year. Internal ice melting accounted for 45% of total ice loss of the 1st year ice, and decreased to 5% of the 10th year ice in summer. Therefore, bottom melting dominated summer melting of MYI when thick snow cover existed.

Overall, snow cover played an important role in the surface radiation heat flux. It changed the ice's thermodynamic evolution and influenced mass balance through the formation of snow ice and superimposed ice. Internal melting may be a potential important factor to affect ice mass balance under global warming, both in Antarctic and Arctic. Ice cores during summer may be effective tool to observe internal ice melting, unfortunately rare related filed work have been conducted before. The systemic observation of internal ice melting is in the future research list now. Snow exists widespread and plentifully in Antarctic, and new study found that Southern Ocean surrounding the continent provided plenty of water vapor to produce heavier snow fall in Antarctic (Yu et al., 2018). Therefore, the knowledge of the snow impact on landfast ice evolution in this study will provide important information for the Antarctic cryosphere community.

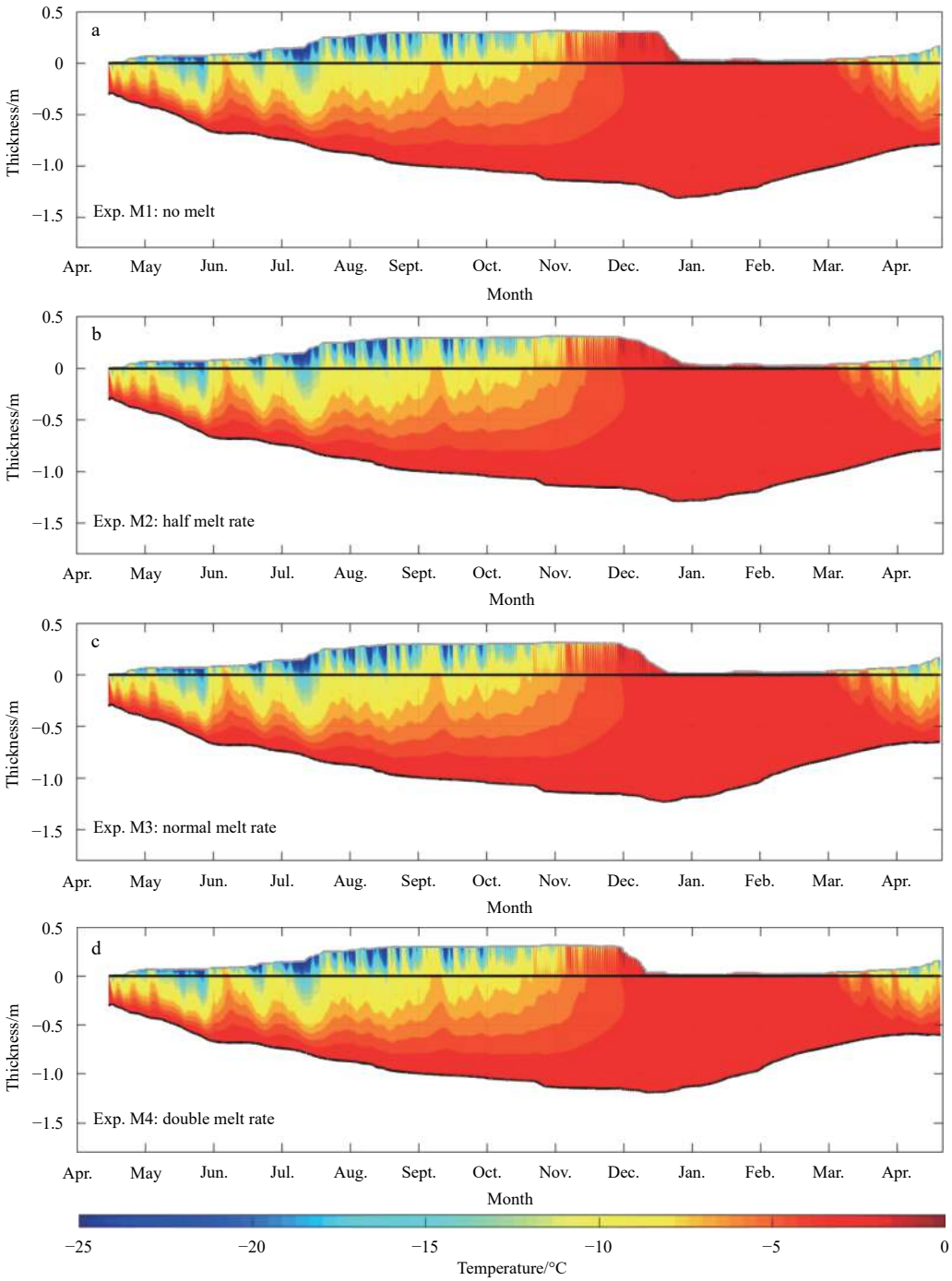

Fig. 11. Sensitivity experiments of different snow melt rate schemes for the onset of surface melt (15 November–15 December): Exp. M1 (a), Exp. M2 (b), Exp. M3 (c), and Exp. M4 (d). The zero position represents the snow/ice interface.

Acknowledgements

We express our highest appreciation to the wintering team of Zhongshan Station, for their contributions to the ice filed observation. We also thank Chinese Arctic and Antarctic Administration (CAA) and Polar Research Institute of China (PRIC), for their well origination and logistical support to the Chinese National Antarctic Research Expedition (CHINARE).

References

Arndt S, Willmes S, Dierking W, et al. 2016. Timing and regional patterns of snowmelt on Antarctic sea ice from passive microwave satellite observations. Journal of Geophysical Research: Oceans, 121(8): 5916–5930, doi: 10.1002/2015JC011504

Briegleb B P, Bitz C M, Hunke E C, et al. 2004. Scientific description of the sea ice component in the community climate system model, version 3. NCAR/TN-463+STR. Boulder, CO, USA: National Center for Atmospheric Research

Cheng Bin, Launiainen J, Vihma T. 2003. Modelling of superimposed ice formation and sub-surface melting in the Baltic Sea. Geophysica, 39(1–2): 31–50

Cheng Bin, Vihma T, Pirazzini R, et al. 2006. Modelling of superimposed ice formation during the spring snowmelt period in the Baltic Sea. Annals of Glaciology, 44: 139–146, doi: 10.3189/

172756406781811277
Cheng Bin, Vihma T, Rontu L, et al. 2014. Evolution of snow and ice temperature, thickness and energy balance in Lake Orajärvi, northern Finland. Tellus A: Dynamic Meteorology and Oceanography, 66(1): 21564, doi: 10.3402/tellusa.v66.21564
Cheng Bin, Zhang Zhanhai, Vihma T, et al. 2008. Model experiments on snow and ice thermodynamics in the Arctic Ocean with CHINARE 2003 data. Journal of Geophysical Research, 113: C09020
Crocker G B, Wadhams P. 1989. Modelling Antarctic fast-ice growth. Journal of Glaciology, 35(119): 3–8, doi: 10.3189/002214389793701590
Heil P. 2006. Atmospheric conditions and fast ice at Davis, East Antarctica: A case study. Journal of Geophysical Research, 111(C5): C05009
Heil P, Allison I, Lytle V I. 1996. Seasonal and interannual variations of the oceanic heat flux under a landfast Antarctic sea ice cover. Journal of Geophysical Research, 101(C11): 25741–25752, doi: 10.1029/96JC01921
Launiainen J, Cheng Bin. 1998. Modelling of ice thermodynamics in natural water bodies. Cold Regions Science and Technology, 27(3): 153–178, doi: 10.1016/S0165-232X(98)00009-3
Lei Ruibo, Li Zhijun, Cheng Yanfeng, et al. 2009. A new apparatus for monitoring sea ice thickness based on the magnetostrictive-delay-line principle. Journal of Atmospheric & Oceanic Technology, 26(4): 818–827
Lei Ruibo, Li Zhijun, Cheng Bin, et al. 2010. Annual cycle of landfast sea ice in Prydz Bay, East Antarctica. Journal of Geophysical Research, 115(C2): C02006
Lynch A H, Chapman W L, Walsh J E, et al. 1995. Development of a regional climate model of the western Arctic. Journal of Climate, 8(6): 1555–1570, doi: 10.1175/1520-0442(1995)008<1555:DOARCM>2.0.CO;2
Maksym T, Markus T. 2008. Antarctic Sea ice thickness and snow-to-ice conversion from atmospheric reanalysis and passive microwave snow depth. Journal of Geophysical Research, 113: C02S12
Massom R A, Drinkwater M R, Haas C. 1997. Winter snow cover on sea ice in the Weddell Sea. Journal of Geophysical Research, 102(C1): 1101–1117, doi: 10.1029/96JC02992
Massom R A, Eicken H, Hass C, et al. 2001. Snow on Antarctic sea ice. Reviews of Geophysics, 39(3): 413–445, doi: 10.1029/2000RG000085
Nicolaus M, Haas C, Willmes S. 2009. Evolution of first-year and second-year snow properties on sea ice in the Weddell Sea during spring-summer transition. Journal of Geophysical Research, 114: D17109, doi: 10.1029/2008JD011227
Parkinson C L, Washington W M. 1979. A large-scale numerical model of sea ice. Journal of Geophysical Research: Oceans, 84(C1): 311–337, doi: 10.1029/JC084iC01p00311
Powell D C, Markus T, Stössel A. 2005. Effects of snow depth forcing on Southern Ocean sea ice simulations. Journal of Geophysical Research, 110: C06001
Tang Shulin, Qin Dahe, Ren Jiawen, et al. 2006. Sea ice characteristics between Middle Weddell Sea and Prydz Bay, Antarctic during the 2003 Australian summer. Earth Science Frontiers (in Chinese), 13(3): 213–218
Yang Yu, Leppäranta M, Cheng Bin, et al. 2012. Numerical modelling of snow and ice thicknesses in Lake Vanajavesi, Finland. Tellus A: Dynamic Meteorology and Oceanography, 64: 17202, doi: 10.3402/tellusa.v64i0.17202
Yang Yu, Li Zhijun, Leppäranta M, et al. 2010. Estimation of oceanic heat flux under landfast sea ice in Prydz Bay, East Antarctica. In: Proceedings of the 20th IAHR International Symposium on Ice. Lahti, Finland, June 14 to 18, 2010
Yang Yu, Li Zhijun, Leppäranta M, et al. 2016a. Modelling the thickness of landfast sea ice in Prydz Bay, East Antarctica. Antarctic Science, 28(1): 59–70, doi: 10.1017/S0954102015000449
Yang Qinghua, Liu Jiping, Leppäranta M, et al. 2016b. Albedo of coastal landfast sea ice in Prydz Bay, Antarctica: Observations and parameterization. Advances in Atmospheric Sciences, 33(5): 535–543, doi: 10.1007/s00376-015-5114-7
Yu Lejiang, Yang Qinghua, Vihma T, et al. 2018. Features of extreme precipitation at Progress Station, Antarctica. Journal of Climate, 31(22): 9087–9105, doi: 10.1175/JCLI-D-18-0128.1
Yu Lejiang, Yang Qinghua, Zhou Mingyu, et al. 2019. The variability of surface radiation fluxes over landfast sea ice near Zhongshan Station, East Antarctica during austral spring. International Journal of Digital Earth, 12(8): 860–877, doi: 10.1080/17538947.2017.1304458
Zhao Jiechen, Cheng Bin, Timo V, et al. 2020. Land-Fast Sea Ice Prediction System (FIPS) for Prydz Bay, East Antarctica: An operational service for CHINARE. Annals of Glaciology, 61(83): 271–283, doi: 10.1017/aog.2020.46
Zhao Jiechen, Cheng Bin, Vihma T, et al. 2019a. Observation and thermodynamic modeling of the influence of snow cover on landfast sea ice thickness in Prydz Bay, East Antarctica. Cold Regions Science and Technology, 168: 102869, doi: 10.1016/j.coldregions.2019.102869
Zhao Jiechen, Cheng Bin, Yang Qinghua, et al. 2017. Observations and modelling of first-year ice growth and simultaneous second-year ice ablation in the Prydz Bay, East Antarctica. Annals of Glaciology, 58(75pt1): 59–67, doi: 10.1017/aog.2017.33
Zhao Jiechen, Yang Qinghua, Cheng Bin, et al. 2019b. Spatial and temporal evolution of landfast ice near Zhongshan Station, East Antarctica, over an annual cycle in 2011/2012. Acta Oceanologica Sinica, 38(5): 51–61, doi: 10.1007/s13131-018-1339-5